Hindawi
Advances in Meteorology
Volume 2022, Article ID 9696174, 14 pages
https://doi.org/10.1155/2022/9696174

Research Article

Influence of Underlying Surface on Distribution of Hourly Heavy Rainfall over the Middle Yangtze River Valley

Yinglian Guo,[1,2] **Jisong Sun**,[2,3] **Guirong Xu**,[1] **Zhiming Zhou**,[1] **and Jizhu Wang**[4]

[1]*Hubei Key Laboratory for Heavy Rain Monitoring and Warning Research, Institute of Heavy Rain, China Meteorological Administration, Wuhan 430205, China*
[2]*State Key Laboratory of Severe Weather, Chinese Academy of Meteorological Sciences, Beijing 100081, China*
[3]*Nanjing Joint Institute for Atmospheric Sciences, Chinese Academy of Meteorological Sciences, Beijing 210000, China*
[4]*Wuhan Central Meteorological Observatory, Wuhan 430074, China*

Correspondence should be addressed to Jisong Sun; sunjs@cma.gov.cn

Received 14 October 2022; Accepted 19 November 2022; Published 21 December 2022

Academic Editor: Hiroyuki Hashiguchi

The variation of boundary layer circulation caused by the influence of complex underlying surface is one of the reasons why it is difficult to forecast hourly heavy rainfall (HHR) in the middle Yangtze River Valley (YRV). Based on the statistics of high-resolution observation data, it is found that the low resolution data underestimate the frequency of HHR in the mountain that are between the twain-lake basins in the middle YRV (TLB-YRV). The HHR frequency of mountainous area in the TLB-YRV is much higher than that of Dongting Lake on its left and is equivalent to the HHR frequency of Poyang Lake on its right. The hourly reanalysis data of ERA5 were used to study the variation of boundary layer circulation when HHR occurred. It can be found that the boundary layer circulation corresponding to different underlying surfaces changed under the influence of the weather system. Firstly, the strengthening of the weather system in the early morning resulted in the strengthening of the southwest low-level air flow, which intensified the uplift of the windward slope air flow on the west and south slopes of the mountainous areas in the TLB-YRV. As a result, the sunrise HHR gradually increases from the foot of the mountain. The high-frequency HHR period of sunrise occurs when the supergeostrophic effect is weakened, the low-level vorticity and frontal forcing are strengthened, and the water vapor flux convergence begins to weaken. Secondly, the high-frequency HHR period of the sunset is caused by stronger local uplift and more unstable atmospheric stratification, but the enhanced local uplift is caused by the coupling of the terrain forcing of the underlying surface and the enhanced northern subgeostrophic flow, which causes the HHR to start closer to the mountain top at sunset than at sunrise.

1. Introduction

Hourly heavy rainfall (HHR), especially extreme HHR, will cause flood, landslide, urban waterlogging, and other disastrous events [1, 2]. A large number of studies have pointed out that the extreme precipitation event around the world has been increasing with global warming [3–5], including the middle Yangtze River Valley (YRV) in China [6–12].

HHR is a result of the interaction among multiscale systems [13–15]. Scientists have analyzed the affecting factors of HHR events from different perspectives. For example, Luo et al. [16] classified the extreme hourly heavy precipitation into four categories according to the synoptic situations in central and eastern China. Shaw et al. [17] and Wang et al. [18] analyzed the effects of surface temperature and humidity on heavy precipitation. Liang and Ding [19] studied the long-term variation of extreme heavy precipitation by the urbanization effect in Shanghai during 1916 to 2014. However, the fine-grained forecast of HHR is still difficult currently since HHR is not only related closely to evolution of multiscale synoptic systems themselves but affected by the boundary forcing from complex terrain or various underlying surfaces. Lock and Houston [20] pointed out that the convection initiation mostly occurred near significant terrain and waters. Guo and Sun [21] analyzed three types of convective systems with different

organizational forms in Hubei Province and found that a large number of nonlinear convective systems may be formed during the movement of isolated convective storms triggered earlier in mountains and hills to plain areas. A large number of studies have shown that the convection triggering and development evolution under different underlying surface conditions are significantly different [22–31]. Therefore, the study on the triggering mechanism of HHR events near multiscale mountains or giant lakes has become an important branch of investigating heavy rainfall.

The diurnal variation of convection triggering and evolution is caused by the difference of underlying surfaces [32]. For example, the bimodal diurnal variation characteristics of HHR frequency in the Yangtze River Valley are a phenomenon different from the unimodal characteristics in most regions of China. As for the formation of bimodal diurnal variation characteristics, it is generally believed that the sunset peak is mainly related to solar radiation heating [33], but there are five views on the causes of the sunrise peak. They are (1) the eastward propagation of the convective system from the Qinghai-Tibet Plateau. However, not all nocturnal convective systems in the Yangtze River Valley move eastward from the east side of the plateau [34, 35]. (2) The mountain-plains solenoid effect [36]. The mountain-plains solenoid effect is a large-scale thermal circulation caused by the three order topography in China, and the solenoid effect of mesoscale mountains on it is lack of investigation. (3) The nocturnal strengthening of low-level jets or boundary layer jets [34, 37–39]. Generally, the appearance time of the strongest jet is mostly earlier than that of the precipitation peak in the early morning, but it is usually considered that early morning was corresponding with the strongest water vapor transport [38]. (4) Locally thermal circulation strengthens the precipitation at night. Generally, the sea-land or lake-land breeze circulation has a more significant enhancement effect on night precipitation, such as the coastal areas of South China [40–42]. In addition, Xue et al. [38] believed that the influence of thermal circulation is not as significant as inertial oscillation in Central China on the early morning HHR events. (5) Convection enhancement was caused by radiation cooling over the cloud top at night [43, 44], but Yin et al. [44] pointed out that it mainly induced night rains in the west of 110°E in China.

To sum up, the reasons for high-frequency HHR at sunrise can be summarized from three perspectives. First, it is caused by movement or propagation of the convection system, as in viewpoint 1. Second, it is induced by the thermal effect, such as viewpoints 2, 4, and 5. Third, it is conducted by the dynamic effect, as in viewpoint 3. The dynamic effect is usually referred to the enhanced convergence and water vapor transport by low-level jets. There are the following views on the reasons for the enhancement of the nocturnal low-level jets: inertial oscillation [45], thermal forcing [46], and a combination of both [47]. In fact, the dynamic effect actually is also closely related to the thermal effect. Du and Chen [48] pointed out that the general low-level jet referred to the jet near 850 hPa, and the 925 hPa or lower jet is called the boundary layer jet. Boundary layer jets can interact with the terrain, so the dynamic and thermal effects of the boundary layer are extremely important for the increase of HHR [49, 50]. Focusing on the complicated mesoscale underlying surfaces around the twain-lake basins, this study will analyze the basic features of the HHR event diurnal variation and the possible effect mechanism. The previous analysis on the causes of high-frequency HHR at sunrise has been relatively comprehensive, but there is no much concern about the causes and evolution of high-frequency HHR at sunset. It is generally believed that it is related to thermal instability. However, the twain-lake basins in the middle YRV (TLB-YRV) have a complex underlying surface, including water bodies, mountains, and plains. The two lakes, Dongting Lake and Poyang Lake, are the largest freshwater lakes in China. Between the two lakes is Mufu-Jiuling Mountain, and Jianghan Plain lies to the northwest of the two lakes. The corresponding HHR characteristics under complex terrain are not consistent. How does the underlying surface affect the distribution and evolution of HHR? The surrounding area of the TLB-YRV is an important food production region and the key transportation hubs of Central China. Therefore, the study of the distribution characteristics and influencing factors of HHR on TLB-YRV underlying surfaces is the basic work to improve the precision forecast of the heavy rain.

The paper is organized as follows: the data and processing methods are introduced in Section 2. Section 3 introduces the characteristics of HHR events around the twain-lake basins, especially the characteristics of diurnal variation. The possible mechanism of affecting temporal-spatial distribution of HHR events around the twain-lake basins are analyzed in Section 4. Section 5 discusses the influence mechanism of the underlying surface. Conclusions are given in Section 6.

2. Data and Methods

2.1. Regional Division. The regional division in this paper is based on the underlying surface attributes. As shown in Figure 1(a), the brown line boxes 1 and 4 are, respectively, Dongting Lake (DT_L) and Jianghan Plain (JH_P) areas, and the corresponding underlying surfaces are, respectively, lake and plain areas. The boundary is mainly based on the lake area and terrain height. Brown line boxes 2 and 3 are Mufu Mountain (MJ_M) and Poyang Lake (PY_L) areas, respectively, and the corresponding underlying surfaces are mountain areas and lake areas, respectively. Based on the terrain height, the junction of mountain areas and lake areas is taken as the boundary between the two areas. The northern boundary of the two areas is the junction of mountain areas and plains, and the southern boundary is the boundary of the middle YRV.

In Figure 1(a), the filled area is the terrain, the blue solid lines are the rivers, the black solid line is the provincial boundary, the brown lines and black numbers indicate subregions (1 = Dongting Lake Area [DT_L], 2 = Mufu-Jiuling Mountainous Area [MJ_M], 3 = Poyang Lake Area [PY_L], and 4 = Jianghan Plain Area[JH_P]), and the red thick solid lines and circled numbers represent the mountains (① = Mufu Mountain and ② = Jiuling Mountain). In

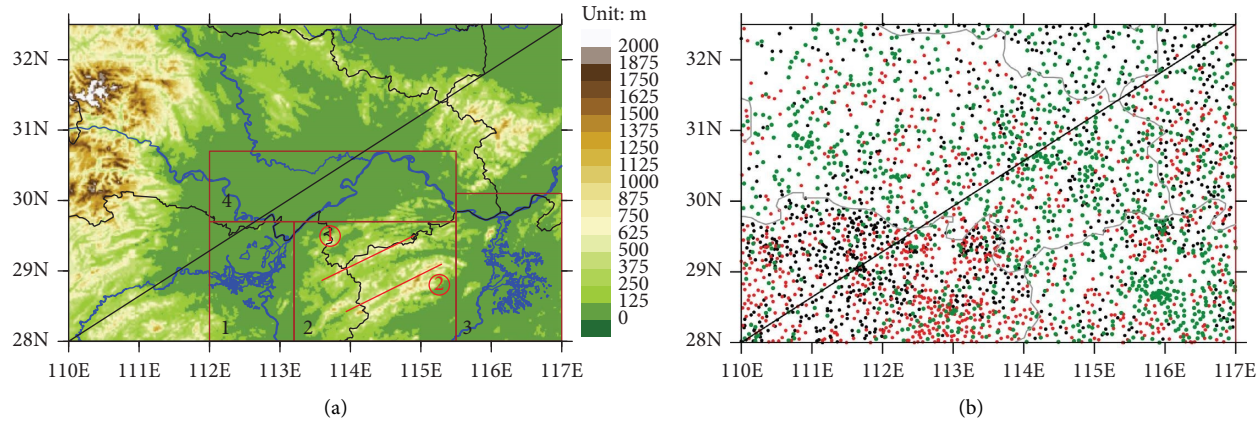

Figure 1: Topography and the location of subregions (a); distribution of ground observation stations (b).

Figure 1(b), black points represent rainfall stations, red points are stations together with rainfall and temperature observation, green points are stations together with rainfall, temperature, and wind observation, and the gray solid line is the provincial boundary.

2.2. Processing of Ground Observation Data. This study collected hourly ground observation data with higher spatial resolution, including national-level and regional-level automatic stations in the middle YRV (28°N–32.5°N, 110°E–117°E) from April to October during 2012–2017. All data are quality controlled using the method of [51], and doubtful data are eliminated. The station whose arrival rate (the ratio of the available record hours to the total observation hours) reaching more than 90% was labeled as an effective observation. In this study, the number of effective rainfall stations reaches to 3109 (Figure 1(b)). The hourly precipitation at any station that reached to 20 mm is recorded as an HHR event [2, 50, 52].

2.3. Definition of HHR Day and Non-HHR Day. During the period from 00:00 to 23:00 (local standard time–LST, the same as follows) of a day, there is at least one HHR at any station in a single subregion. This day is defined as the HHR day of the subregion. For Non-HHR days, it is required that the stations in the four subregions in Figure 2 do not have HHR within 24 hours on a certain day, hereinafter referred to as NONE.

2.4. Processing of Atmospheric Background Data. The ERA5 global reanalysis data (horizontal resolution 0.25° × 0.25°, with hourly temporal resolution) were used to investigate atmospheric evolution. The hourly average fields of the HHR days in each subregion are called JH_P: ave, DT_L: ave, MJ_M: ave, and PY_L: ave. The hourly average fields of the HHR days in all subregions (excluding the same date in each subregion) are called as ALL: ave. In order to analyze the relevant characteristics of the two peak periods of HHR daily variation: sunrise (05:00 to 09:00) and sunset (16:00 to 18:00), the composite mean field of the corresponding periods

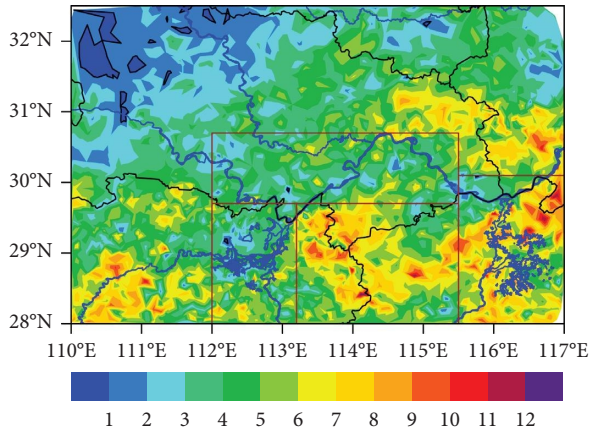

Figure 2: Annual average distribution of the HHR frequency in the middle YRV from April to October 2012-2017. The brown lines indicate partitions, the same as Figure 1(a).

of HHR days in each subregion (JH_P, DT_L, MJ_M, and PY_L) is calculated and called JH_ P:sunrise, DT_ L: sunrise, MJ_ M: sunrise, PY_ L: sunrise, JH_ P:sunset, DT_ L: sunset, MJ_ M: sunset, and PY_ L: sunset.

3. Characteristics of HHR Frequency

3.1. Spatial Distribution of HHR Frequency. From the annual average frequency of HHR events in the middle YRV from April to October during 2012–2017 (Figure 2), the following facts can be found: (1) the frequency distribution in the middle YRV showed more HHR events in the southeast and fewer in the northwest. PY_L and MJ_M are the two regions with the highest-frequency HHR events. This is slightly different from the results of Chen et al. [53] only using the national stations analysis. Chen et al. [53] indicated that DT_L and PY_L were high-frequency areas of HHR events, and the frequency in MJ_M was not only lower than in PY_L but was even lower than in DT_L. This should be caused by scattering data used in their investigation, and the mesoscale features of HHR events in the complex terrain region were impossible to be exposed well by scattering national stations.

(2) There were significant differences in the frequency of HHR events between the two giant lakes (Dongting Lake (DT_L) and Poyang Lake (PY_L)), which are the two largest lakes with similar latitude in the middle YRV. Most HHR activities appear around PY_L, and the lowest frequency of HHR events occurs in DT_L area. This may be closely related to differences in topographic distribution around the two lakes. The surrounding area of DT_L is relatively flat, its west and south sides are relatively far away from the mountains, and its north side is adjacent to Jianghan Plain. However, the surrounding terrain of PY_L is much more complex, similar to a basin, with some small hills scattered around it. (3) The frequency distribution in MJ_M was closely related to the mountains. The two high-frequency bands in MJ_M were located, respectively, in the western side of Mufu-Jiuling Mountain and along the Jiuling Mountain. (4) The frequency of HHR events in JH_P is much lower than that in PY_L and MJ_M, but the Dabie Mountain on the north side of JH_P and PY_L is a high-frequency area of HHR events. Fu et al. [34] studied the relationship between high-frequency HHR in the early morning of the Dabie Mountains and the low-level jet in the boundary layer and pointed out that the high-frequency HHR was related to the inertial oscillation of low-level jets. The terrain of the Dabie Mountain is along northwest-southeast direction, almost perpendicular to the southwest jet. The lifting mechanism in the windward slope was considered to play an important role in the early morning HHR of the Dabie Mountains. However, the terrain of Mufu Mountain is along the southwest-northeast direction, parallel to the southwest jet, and the influence of the underlying surface increases the influence of the water body. Are the temporal and spatial distribution and diurnal variation features of HHR events affected by local circulation? Is there any interaction between local circulation and weather system?

3.2. Diurnal Variation of the HHR Frequency. The difference of temperature, humidity, and turbulence caused by solar radiation on different underlying surfaces results in the local circulation of the boundary layer and its diurnal variation. By statistical analysis of the diurnal variation characteristics of the HHR events in the four subregions (Figure 3), it is found that there are bimodal diurnal variation characteristics of HHR frequency in each subregion. The diurnal variation of HHR event frequency over the PY_L and MJ_M presents obviously bimodal characteristics, and the two peaks appear at 17:00 at sunset and about 06:00 at sunrise. This is consistent with the diurnal characteristics of the middle-lower reaches of the Yangtze River Valley investigated by Yu et al. [11, 12]. Generally, the most unstable atmospheric stratification appears in the afternoon, so the peak time of HHR frequency at sunset is essentially the same as the thunderstorm or gale event frequency in this region [21]. The peak of HHR event frequency at sunrise is related to the interaction between local circulations and the synoptic system. However, DT_L and PY_L are, respectively, located in the east and west of MJ_M. The bimodal diurnal variation around PY_L is significant, while the bimodal feature

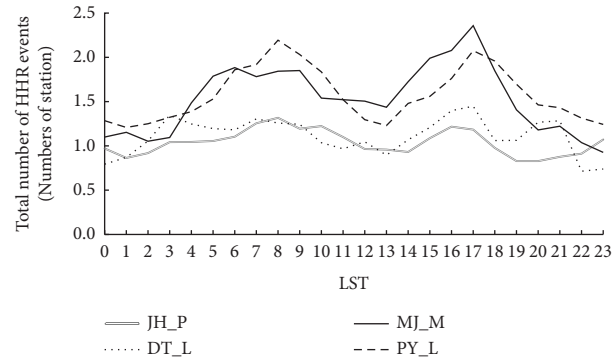

Figure 3: Diurnal variation of HHR event frequency over the four regions (JH_P, DT_L, MJ_M, and PY_L) around the TLB-YRV. The ordinate axis represents the ratio between the total number of HHR events in the subregion and the number of stations in the subregion, and the abscissa axis represents hours in a day.

around DT_L is relatively insignificant. The bimodal characteristics around JH_P are not significant as DT_L. This is related to the lower HHR frequency in these two regions.

In order to clarify the relationship between the frequency of HHR events and the underlying surface environments, Figure 4 shows the hourly distribution and topography of the HHR events around the TLB-YRV. At MJ_M area, the spatial distribution and evolution of high-frequency HHR events (red dots) at sunrise are different from those at sunset. At sunrise, high-frequency HHR first occurs on the northwest slope and then gradually extends to the whole MJ_M area. At sunset, high-frequency HHR erupts along the ridge of Mufu Mountain and usually spreads to the surrounding areas with a fast decreasing frequency. As shown in Figure 4, the number of stations with high-frequency HHR events increased rapidly around 05:00 on the northwest slope of Mufu Mountain and reached the maximum at 06:00, which corresponds to the sunrise peak at 06:00 in Figure 3. At 08:00–09:00, the high-frequency stations are relatively well distributed over Mufu Mountain and Jiuling Mountain. After 10:00, the number of high-frequency stations is significantly reduced. At 16:00, the number of high-frequency HHR stations in the western Mufu Mountain increased rapidly again. The high-frequency stations were more concentrated and closer to the ridge of Mufu Mountain than at 06:00. After 18:00, the number of high-frequency stations decreases obviously, and the distribution gradually tends to disperse. In the late evening (until 23:00), the number of high-frequency stations decreased more slowly than in the morning, which seems inconsistent with Figure 3. This is because the frequency of HHR events is much higher during 16:00–17:00 than that in later evening over the MJ_M area.

In PY_L area, the evolution of high-frequency HHR events during sunrise and sunset is in good agreement with the lake-land breeze circulation; that is, the high-frequency HHR at sunrise extends outward from the center of the lake, and the high-frequency HHR at sunset spreads from mountains to the center lake. As shown in Figure 4, during 06:00–10:00, stations with the high-frequency HHR events are mainly distributed on the northeast and southwest of the

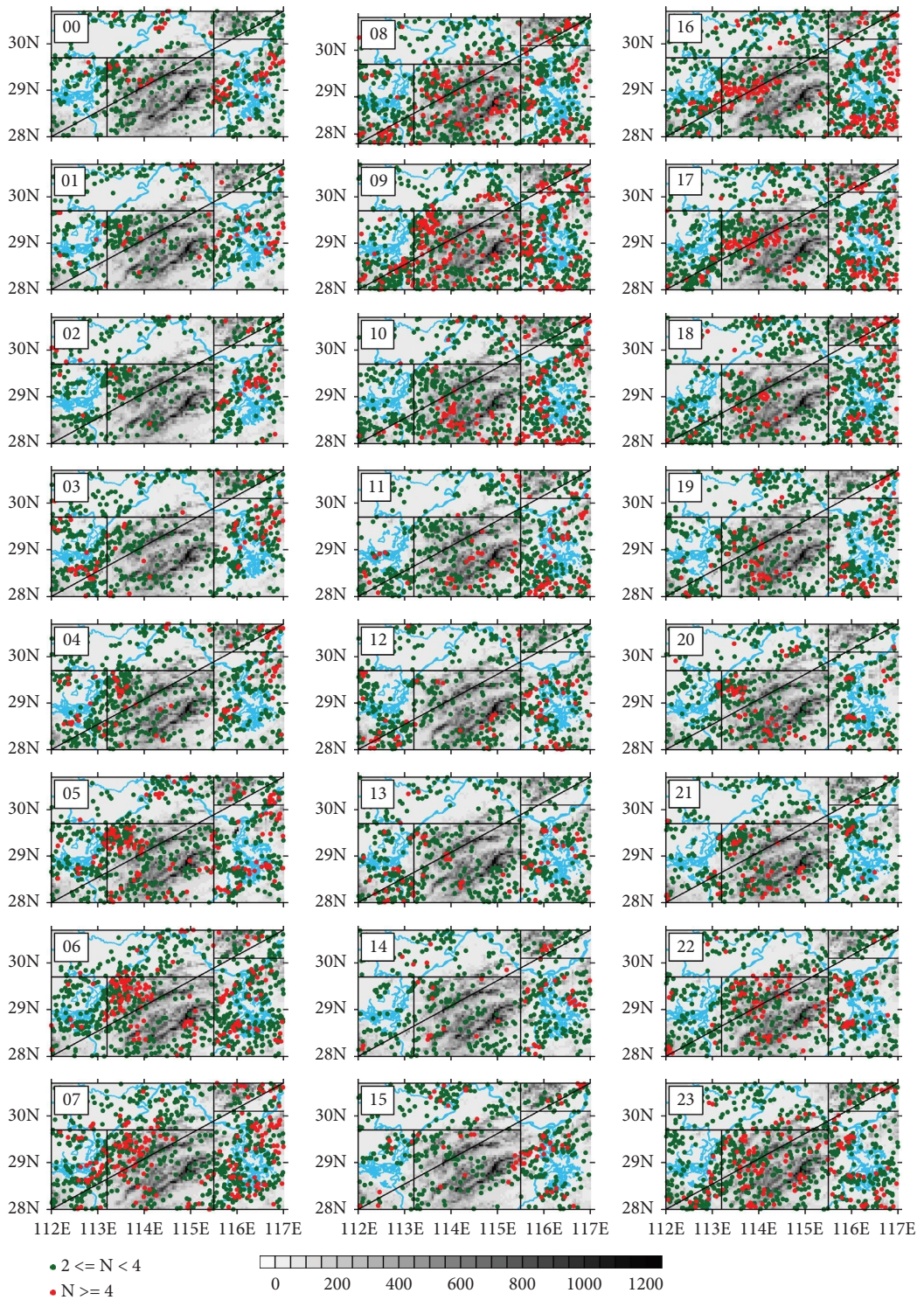

Figure 4: Hourly distribution of HHR event frequency of each station (the number in the upper left corner is local standard time, the filling is terrain, the blue line is river and lakes, and the color dots represent the HHR event frequency of each station, where the red dots represent high-frequency events).

Poyang Lake. Most of the stations with the high-frequency HHR events on the southwest are closer to Poyang Lake than to Jiuling Mountain. It is easy to find from Figure 4 that the distribution evolution of the stations with high-frequency HHR events initially appears near the lake center (during 05:00–06:00) and then gradually expanded outward. Another frequency peak of HHR events over PY_L appears in the afternoon to evening. The stations with high-frequency HHR events over PY_L first appear along the northwest bank of the Poyang Lake (15:00) near Jiuling Mountain and

then spread around the lake and locate away from mountains. The number of the stations with high-frequency HHR events reaches the peak at 16:00–17:00, which is consistent with Figure 3. Comparing the evolution trends of the two high-frequency HHR periods of sunrise (05:00~08:00) and sunset (15:00~17:00), it can be found that the stations with high-frequency HHR events during the sunset period are stably distributed around the lake, and there is no high-frequency station similar to the sunrise near the central lake.

In DT_L, different from PY_L, the stations with the high-frequency HHR events are mainly concentrated on the south side of the Dongting Lake whether in morning or afternoon-evening. The number and density of the stations with high-frequency HHR events over the DT_L region are much less than over PY_L, and the diurnal variation amplitude of HHR event frequency is also the lowest in the three regions.

4. Possible Mechanism of Underlying Surfaces on HHR Events

The previous analysis shows that the frequency of HHR events around the TLB-YRV exhibits a bimodal diurnal variation, but amplitudes of the diurnal variation in the DT_L and JH_P are much smaller than that in MJ_M and PY_L. In mountain and lake areas, the location and movement trend of high-frequency HHR events in the morning and evening are also different. The previous phenomena may be related to the following mechanisms: (1) diurnal variation of the HHR weather system and (2) local circulation of the boundary layer caused by difference of the underlying surface.

4.1. Diurnal Variation of the Boundary Weather System. The highest altitude of Mufu-Jiuling Mountains is lower than 1500 m, and the direct interaction between the weather system and the underlying surface is mainly under 850 hPa. Figure 5 shows the 925 hPa synthetic wind fields and θ_{se} when HHR events occur in four subregions (JH_P, DT_L, MJ_M, and PY_L), respectively. It is easy to be found that their boundary layer weather control systems are similar, but the HHR events in each subregion occur in different positions of the system. This means that most HHR events in the middle YRV are caused by medium-α-scale vortex or horizontal wind shear. This is consistent with the development of mesoscale vortex systems or wind shears in the lower troposphere during Mei-Yu period in the YRV [54–57], and the monthly average frequency of HHR events over the twain-lake basins indicated that most of HHR events happened during June to July (the figure omitted) and were corresponding with the Mei-Yu season.

The boundary layer circulation of non-HHR roughly represents the local climate characteristics in warm seasons. The HHR diurnal variation minus the non-HHR diurnal variation can remove the regular diurnal variation of the boundary layer flow field so as to better reveal the diurnal variation of the weather system with HHR. Of course, it still includes the influence of the weather system on the boundary layer circulation. Figure 6 shows the regional average diurnal variation of vorticity and vapor-flux divergence on HHR days minus non-HHR days, where the regional average range is 28°N–30.7°N, 112°E–117°E. It includes the three key subregions (DT_L, MJ_M, and PY_L) of TLB-YRV. The maximum value of vapor flux convergence (-1.1×10^{-7} g kg^{-1} s^{-1}) in Figure 6 appears during 01:00–06:00 under 950 hPa with the warm-wet low-level jet strengthening after midnight, and vorticity of the synoptic system reaches maximum (more than 1.7×10^{-5} s^{-1}) during 07:00–10:00 at 900 hPa. In the afternoon, the subgeostrophic effect causes reducing of the vortex system and vapor flux convergence at low levels in the afternoon, and the central value of vapor flux convergence goes down to -6×10^{-8} g kg^{-1} s^{-1} during 13:00–16:00, and the convergence stars to enhance slightly again in the evening (about 17:00) at this level.

The previous analysis shows that the HHR boundary weather system presents diurnal variation features: HHR events at sunrise are related with vorticity strengthening and appear after vapor flux convergence up to maximum. However, the high-frequency HHR events at sunset are impossible to be well explained by the diurnal variation of the synoptic system itself since the highest-frequency HHR events are corresponding with only slight increase of vapor flux convergence and no obviously enhancement of vorticity at low levels. On the other hand, the diurnal variation of the weather system cannot explain the different diurnal variation behaviors of the HHR events in mountain and lake areas. This implies that the local circulations caused by the complex underlying surface may play another important role in affecting the diurnal variation of the subregions HHR events around TLB-YRV.

4.2. Impact of the Underlying Surface. First, from the average divergence/convergence at 925 hPa and surface flow on the non-HHR days (Figure 7), it can be found that the mountain-valley breeze caused by the MJ_M is the clearest boundary local circulation in the TLB-YRV. The mountain breeze at sunrise corresponds to the divergence at 925 hPa, and the valley breeze at sunset corresponds to the convergence at 925 hPa. The height of the lake-land breeze near the lake area is lower than that of the mountain-valley breeze because the land breeze in the morning (converging to the lake center) and the lake breeze in the evening (divergent to the lake shore) are clear near the surface, but the divergence of 925 hPa above the twain-lake basins is always greater than 0, especially at DT_L. At sunrise (Figure 7(a)), the convergence zone by mountain breeze is located along the south-eastern and western slopes of MJ_M over 925 hPa, and the strongest convergence center (-1.5×10^{-5} s^{-1}) is along the western slope of MJ_M or the eastern side of DT_L. This indicates that the mountain breeze is more conducive to strengthening the convergence and uplifting movement on the west side of MJ_M, and its position is consistent with the location of the high-frequency HHR events in the early morning. At sunset, the thin lake breeze,

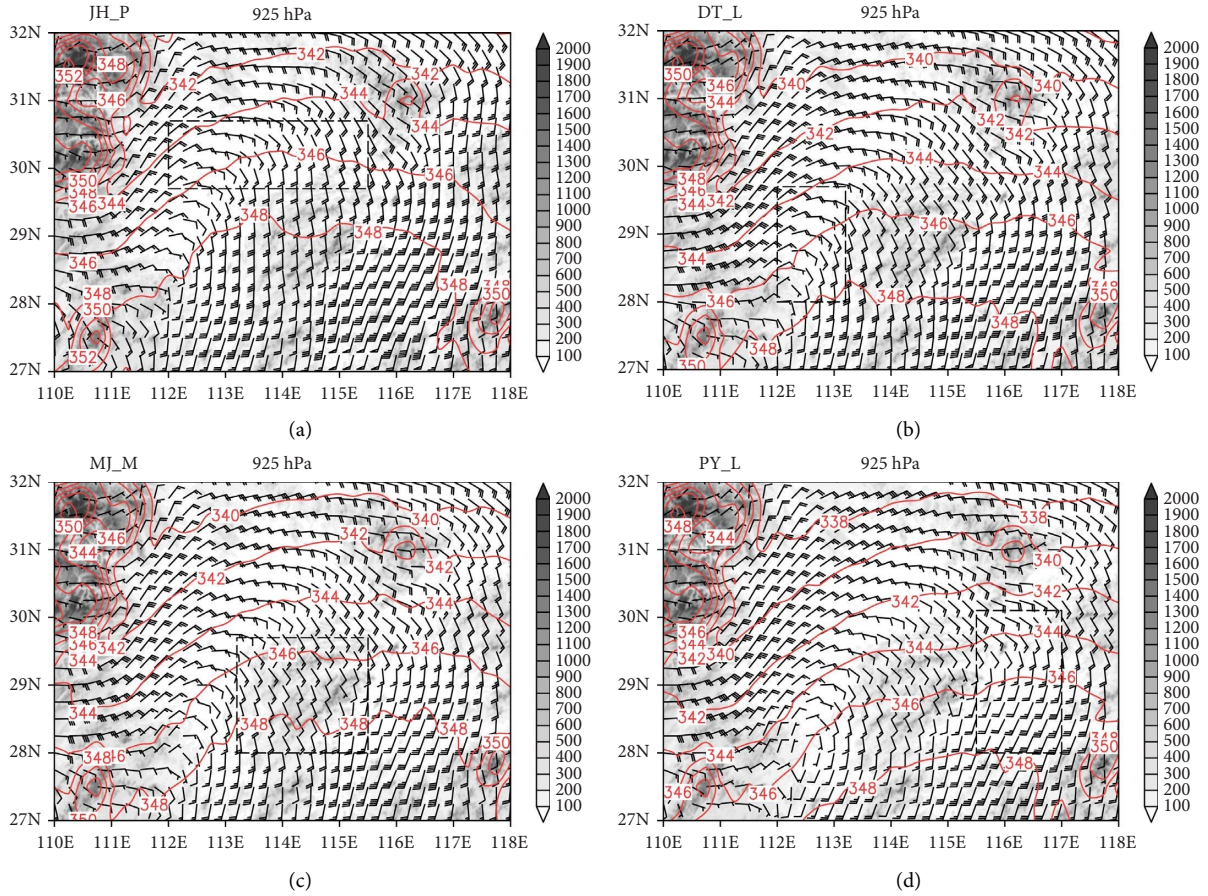

FIGURE 5: Synthesized wind (barb; m·s^{-1}; each bar for 1 m·s^{-1}) and θ_{se} (red solid line; K) at 925 hPa when HHR events occur in different subregions (a) JH_P, (b) DT_L, (c) MJ_M, and (d) PY_L, respectively. The black dashed line box is the respective HHR area, and the gray fill is the terrain altitude (m).

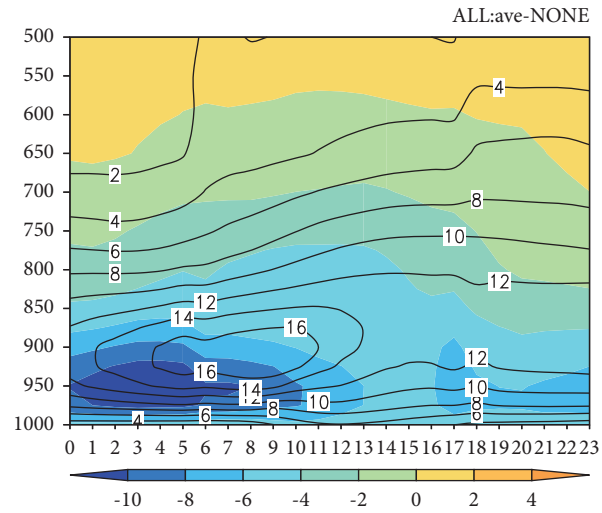

FIGURE 6: Regional (28°N–30.7°N, 112°E–117°E) average diurnal variation of vapor-flux convergence (color, 10^{-8} g kg^{-1} s^{-1}) and vorticity (black line, 10^{-6} s^{-1}).

which is guided by DT_L and PY_L on both sides of MJ_M, is favorable for intensifying the valley breeze and induces stronger convergence toward the mountain top. The superposition effect of mountain-valley breeze and lake-land breeze leads to the convergence intensity of the mountain top at sunset (the maximum convergent

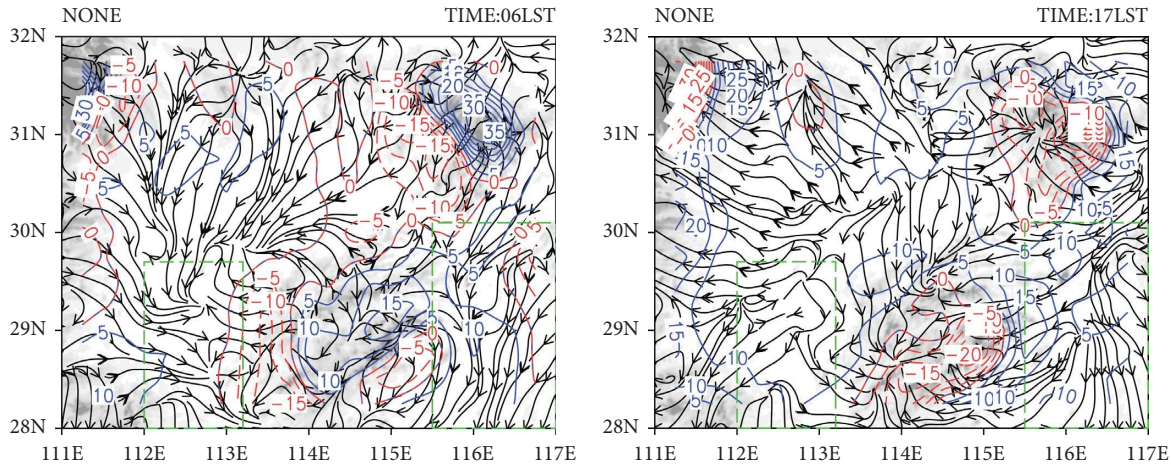

Figure 7: The average divergence at 925 hPa (the red line represents convergence, the blue line represents divergence, and the unit is $10^{-6}\,s^{-1}$) and surface flow (stream) at 06:00 (a) and 17:00 (b) on non-HHR days.

intensity in 925 hPa reaches $-2.0\times10^{-5}\,s^{-1}$) is stronger than that along the slope at sunrise (convergent intensity is down to $-1.5\times10^{-5}\,s^{-1}$).

Then, we analyze the divergence/convergence at 925 hPa and surface flow on HHR days (Figure 8). Considering that 02:00 and 14:00 are the least active periods of HHR events (Figure 3), the low-level flow and divergence at these two time points can maximally avoid the feedback effect of HHR events on local circulation and can better reveal the characteristics of boundary layer circulation under the action of HHR weather systems. It can be seen from Figure 8 that the patterns of average surface flow and divergence in 925 hPa at 02:00 of the HHR days (Figure 8(a)) are roughly similar to that of Figure 7(a). The land breeze convergence over DT_L region is clearer. There is a stronger convergence (the minimum value is less than $-2.0\times10^{-5}\,s^{-1}$) around MJ_M slopes, and there is a more intense divergence (the maximum value reaches up to $2.5\times10^{-5}\,s^{-1}$) at mountaintop over 925 hPa. Figure 8(b) is similar to Figure 7(b), MJ_M is covered by local convergence in 925 hPa at 14:00 (Figure 8(b)), and their intensities are roughly similar. However, due to the influence of the HHR weather system, northerly wind prevails on the ground in the middle YRV. The surface flow field on the top of the mountain is even dominated by downslope wind (similar to mountain wind), but the convergence area of MJ_M at 925 hPa is obviously larger than that in Figure 7. It can be seen that the weather system conducive to HHR events has not fundamentally changed the pattern of divergence and convergence around MJ_M at sunrise and sunset, but they are significantly strengthened.

Last, Figure 9 shows the deviation (HHR days of each subregion minus non-HHR days) vertical sections (along 29°N) of θ_{se} and divergence. It can be found that no matter which subregion is hit by the HHR event, the deviation patterns of θ_{se} and divergence in the vertical sections along 29°N are slightly similar. Corresponding with the peak of HHR events frequency at sunrise, a clearly and distinguishably slant front under 850 hPa distributes from west (cold) to east (warm) with a high θ_{se} zone over the slant front. On the contrary, there is not obviously a horizontal gradient of θ_{se} in the low-level troposphere around MJ_M at sunset. It is furtherly confirmed that the high-frequency HHR events at sunrise are guided by the intensifying nocturnal synoptic system, which not only presents vorticity and vapor-flux convergence strengthening but also represents front forcing to be intensified. In addition, the west side of MJ_M, as the windward slope of the southwest low-level jet, is affected by the supergeostrophic effect before sunrise, which enhances the convergence enhancement of the west side of MJ_M, resulting in stronger rising than that of non-HHR days. The deviation of the conditional static stability ($\partial\theta_{se}'/\partial p>0$) of the troposphere below 750 hPa in the MJ_M region shows that it is more unstable at sunset than at sunrise, indicating that local uplift plays a decisive role in triggering the convective high-resolution high-frequency HHR event at sunset. It shows that the local lifting plays a decisive role in triggering the high-frequency HHR events at sunset. The differences of the stratification status and trigger mechanism induce the variation of convective intensity at sunrise and sunset. It can be confirmed by some features of radar reflective intensity, which correspond to the two peak periods of HHR events in MJ_M, respectively (Figure omitted). For example, the average height of maximum radar reflective intensity of high-frequency HHR events at sunset is higher than that at sunrise (3.01 km vs 2.76 km), and the average thickness of radar reflective intensity above 40 dBZ at sunset is thicker than that at sunrise (1.55 km vs 1.26 km). In conclusion, the strong convergence movement at sunset cannot be directly caused by the weak weather system itself but may be caused by the topographic forcing caused by the underlying surface and the thermal circulation in the boundary layer. In addition, it is worth noting that (1) when HHR occurs in any subregion, the slant convergence is well matched from the eastern side of MJ_M to the western shore of PY_L, but their intensities present obviously

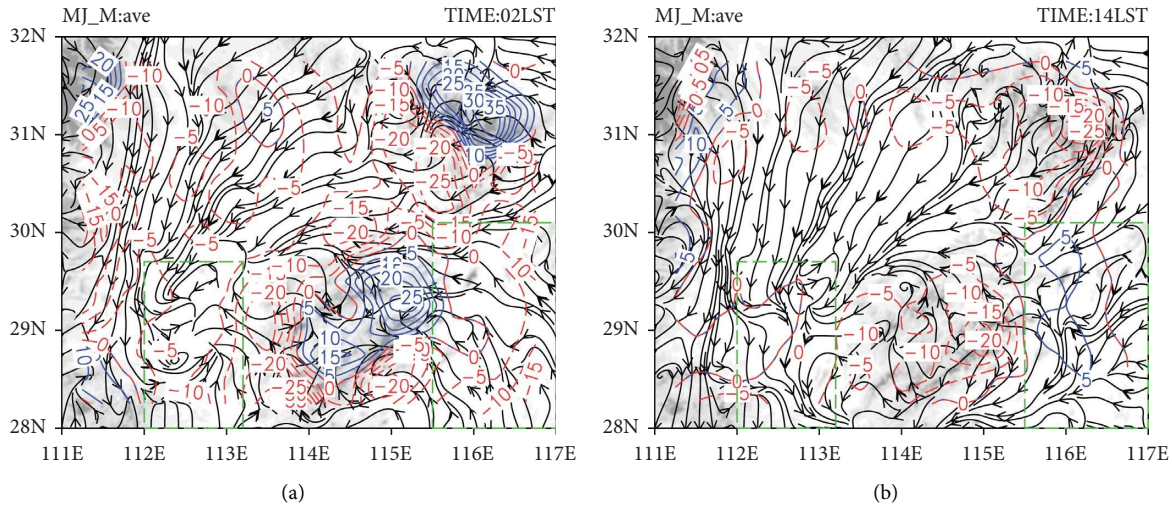

Figure 8: The same as Figure 7 but at 02:00 (a) and 14:00 (b) on the HHR days in MJ_M.

different in the western slope of MJ_M when the HHR events happen in different subregions. (2) Below 800 hPa, the conditional static stability between PY_L and MJ_M is more unstable than that between DT_L and MJ_M. It implies that corresponding to the HHR synoptic system, the local convergence intensity and unstable stratification in the east of MJ_M are more remarkable than those in the west, and more convective HHR events are induced near the top of MJ_M and along the lakeshore of PY_L at sunset.

5. Discussion

Generally, the intensifying low-level airflow caused by inertial oscillation is considered to be a significant forcing factor to induce nocturnal heavy rainfall [38, 40]. The oscillation nature of low-level airflow is thought as a result of the diurnal variation of the turbulence intensity [41, 45]. The supergeostrophic wind appears after midnight with turbulence weakening under the boundary layer, and the wind vector rotates clockwise and induces the vorticity and low-level jet to be intensified. On the contrary, the enhancing turbulence induces the subgeostrophic effect in the afternoon. Hourly ERA5 data can well show the diurnal variation characteristics of inertial oscillation and have a certain reproducibility ability for the mountain-valley breeze or lake-land breeze in the study area of this paper. However, it is still difficult to quantitatively separate the diurnal variation of wind field caused by inertial oscillation from the thermal circulation in the boundary layer, so geostrophic wind is used to analyze them together. The ageostrophic flow can well represent divergence/convergence, so the analysis of the ageostrophic flow on different underlying surfaces can explain the action mechanism of the topographic forcing caused by the underlying surface and the boundary layer thermal circulation on HHR.

Figures 10(a)–10(d) shows the diurnal variation (hourly value minus daily average value) of the ageostrophic wind when HHR occurs at sunrise or sunset in each region, and Figure 10(f) shows the diurnal variation of the ageostrophic wind on non-HHR days. It is easy to find that whether on HHR days or non-HHR days, the diurnal variation direction of the low troposphere ageostrophic wind has obvious inertial oscillation characteristics (clockwise rotation with time). The diurnal variation amplitude of the ageostrophic wind in non-HHR days is weaker than that in any subregion with HHR events. In non-HHR days, the maximum supergeostrophic wind (southwestern wind less than $1.5\,\mathrm{m{\cdot}s^{-1}}$) from midnight to early morning occurs near 875 hPa, and the strongest subgeostrophic wind (northern wind less than $1.5\,\mathrm{m{\cdot}s^{-1}}$) appears near 950 hPa from afternoon to evening. Compared with the regional ageostrophic wind of the non-HHR days, the average ageostrophic wind of HHR days in MJ_M and PY_L shows bigger amplitude of diurnal variation either HHR events at sunrise or sunset. The strongest supergeostrophic phenomenon induces more a powerful southwest low-level jet at midnight, and the strongest subgeostrophic (northern wind) that appears in the evening significantly reduces the prevailing southern flow. Corresponding to HHR days, the subregional average velocity of the maximum ageostrophic (regardless of supergeostrophic or subgeostrophic) wind over MJ_M is stronger than that over PY_L, and their difference is about 0.2 m/s. It indicates that the terrain is not only conducive to the strengthening low-level jet at midnight but also its friction effect is more favorable for producing a subgeostrophic effect in the evening. It is also worth noting that the strong subgeostrophic wind occurs from 18:00 to 19:00, which is about 1–2 hours later than the sunset peak time (16:00–17:00) of HHR frequency. This means that more HHR events in evening occur during the stage of the subgeostrophic wind strengthening, instead of the strongest subgeostrophic period. More HHR events in the early morning (05:00~09:00) occur in period of the low-level supergeostrophic wind weakening (Figure 10) or the low-level vertical vortex gradually intensifying (Figure 6). The mechanism may be related to the convergent forcing caused by the ageostrophic effect.

The vertical vorticity tendency equation without the advection term is as follows:

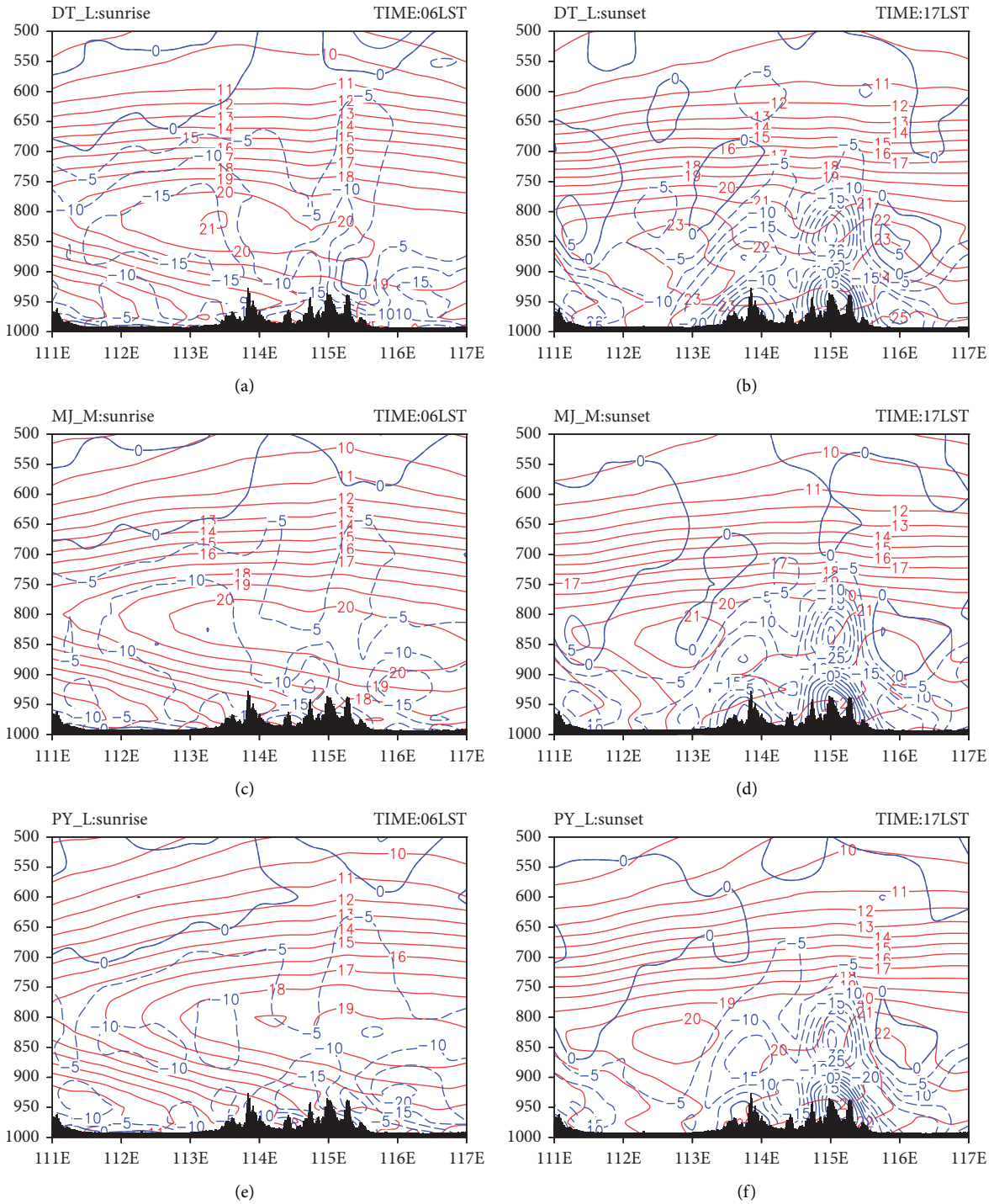

Figure 9: The deviation (HHR days of each subregion minus non-HHR days) vertical sections (along 29°N) of divergence (blue line; $10^{-6}\,s^{-1}$) and θ_{se} (red line; K).

$$\frac{\partial \zeta}{\partial t} = -fD' + \left(\frac{\partial F_x}{\partial x} - \frac{\partial F_y}{\partial y}\right). \quad (1)$$

Among them, $\zeta = (\partial v/\partial x) - (\partial u/\partial y)$ is the vertical vorticity of horizontal full wind speed; $D' = (\partial u'/\partial x) + (\partial v'/\partial y)$ is ageostrophic divergence, where $v' = v - v_g, u' = u - u_g$ are ageostrophic wind, and F_x, F_y is friction.

The role of the topographic friction will be briefly discussed first. On the northeast side of the Dongting Lake, the west-east direction is the transition zone from lake area to mountainous area $(\partial F_x/\partial x) > 0)$, and its north is from the mountainous area to the plain $(\partial F_y/\partial y) < 0)$; meanwhile, the south is from the mountainous area (north slope of Xuefeng Mountain) to the lake area $((\partial F_y/\partial y) < 0)$, so the topographic friction effect is favorable for the local vorticity

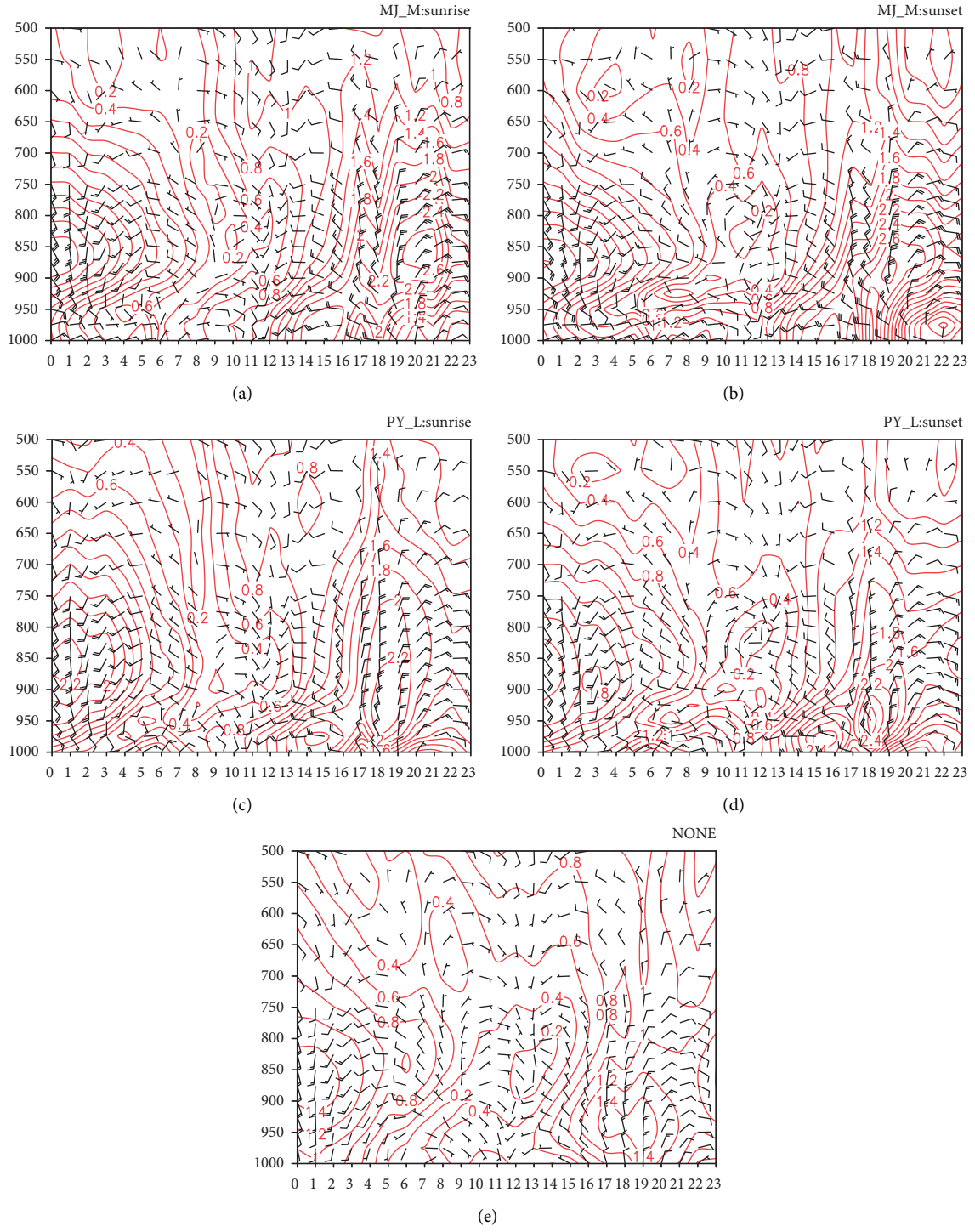

FIGURE 10: The diurnal variation (hourly value minus daily average value) of the ageostrophic wind when HHR occurs at sunrise or sunset in each region (Figure 10a-d) and the diurnal variation of the ageostrophic wind on non-HHR days (Figure 10e). The regional average range of Figure 10e is (27°N–32°N, 110°E–118°E), and the regional average range of other figures is marked in the upper right corner. The contour line represents the wind speed, and one bar of wind bar is 1 m/s.

to be enhanced over the DT_L area. This may be the reason about why the average location of the low-level vorticity center is generally located near DT_L, regardless of HHR events happening in any subregion (Figure 5). The topographic friction effect is an important forcing mechanism on more HHR events either in early morning or evening to likely start on the south of DT_L and northwest slope of MJ_M.

The diurnal variation of the low-level divergence by ageostrophic wind is another important mechanism which

induces the diurnal variation of the HHR events. In the early morning $v' > 0$, the enhancement of vorticity always follows the stronger convergent movement in low levels. This can be confirmed by the sequential evolution of the vapor flux convergence and vorticity (Figure 6). In the evening, $v' < 0$ with the negative ageostrophic vorticity ($\zeta' < 0$), the enhancement of the low-level convergence induces the positive vorticity of assembling wind speed to weaken slightly with quickly increasing the HHR station numbers during 16:00–17:00 (Figures 6 and 4). On the other hand, in correspondence with HHR events at sunset either in MJ_M or PY_L, the maximum absolute value of the average subgeostrophic wind in low levels is larger than that at sunrise (the differences is about 0.2~0.4 m/s), and it indicates that the stronger subgeostrophic acceleration is favorable for triggering HHR events in the evening.

6. Conclusions

In this study, the hourly surface observation data with higher spatial resolution and ERA5 reanalysis data from April to October during 2012–2017 in the middle YRV were used to investigate the fundamental characteristics of HHR events around the twain-lake basins and their possible mechanisms, such as the temporal-spatial distribution, diurnal variation, and the complicated interactions among the favorable synoptic system, the locally mesoscale topography, and lake-land circulation. Results indicate

(1) PY_L area and MJ_M area are regions of the high-frequency HHR events in the middle YRV. As the two largest lakes in the region, DT_L and PY_L locate at similar latitude and, respectively, in two sides of MJ_M, but the most active HHR events appear around PY_L and the lowest frequency of HHR events over DT_L in the region. Other high-frequency HHR events distribute in MJ_M, and this is different from the statistic results based only on sparse national stations. Some previous studies considered that the frequency of HHR events in MJ_M was not only lower than over PY_L but even lower than over DT_L. The investigation finds that there are two high-frequency bands over MJ_M: one of them is located along the northwest slope of Mufu Mountain, and another presents basically along Jiuling Mountain and extends to the west bank of the PY_L. The frequencies of HHR events in subregions of the middle YRV almost all present bimodal diurnal variations but with different amplitude. PY_L or MJ_M shows a significant bimodal characteristic, with two peaks at sunset (about 17:00) and sunrise (about 6:00). The hourly location evolution of HHR events display that the initial location of the high-frequency HHR events over MJ_M is closer to the mountain top in the evening than in the early morning. The high-frequency stations of HHR events around PY_L in the evening locate further away from the center of the lake than in the early morning.

(2) The ageostrophic effect of air flow in low levels is possible to be an important mechanism which induces the diurnal variation of the HHR events. The high-frequency HHR events in early morning are guided by nocturnal intensification of the favorable synoptic system, and HHR events appear in the stage of the supergeostrophic effect weakening and the vapor flux convergence going down from the maximum, which is in correspondence with vertical vorticity and front forcing strengthening at low levels. On the other hand, the convergent lifting is intensified in the west and south slope of MJ_M by strengthening low-level south-westerly with supergeostrophic flow, and their synergic effect induces more HHR events to start along the two slopes of MJ_M in the early morning. The high-frequency HHR events in the evening are led by the local lifting trigger with more unstable atmospheric stratification and the diurnally weakening synoptic system. Strengthening local lifting is conducted by the coupling effect of terrain forcing and intensifying northern subgeostrophic flow, and it induces more HHR events to begin near the ridge of MJ_M in the evening than in the early morning.

Data Availability

The Chinese Academy of Meteorological Science provides the national stations and regional automatic stations' data in China. ECMWF datasets provide the ERA5 Global Reanalysis Data. (https://cds.climate.copernicus.eu/cdsapp#!/dataset/reanalysis-era5-pressure-levels?tab=overview).

Conflicts of Interest

All authors declare that they have no conflicts of interest.

Acknowledgments

This study was supported by the National Key Research and Development Program (2018YFC1507200).

References

[1] C. A. Doswell, H. E. Brooks, and R. A. Maddox, "Flash flood forecasting: an ingredients-based methodology," *Weather and Forecasting*, vol. 11, no. 4, pp. 560–581, 1996.

[2] J. Sun, "Differences and relationship between flash heavy rain and heavy rainfall," *Torrential Rain and Disasters*, vol. 36, no. 6, pp. 498–506, 2017.

[3] P. Berg, C. Moseley, and J. O. Haerter, "Strong increase in convective precipitation in response to higher temperatures," *Nature Geoscience*, vol. 6, no. 3, pp. 181–185, 2013.

[4] E. M. Fischer and R. Knutti, "Observed heavy precipitation increase confirms theory and early models," *Nature Climate Change*, vol. 6, no. 11, pp. 986–991, 2016.

[5] G. Lenderink and E. Van Meijgaard, "Increase in hourly precipitation extremes beyond expectations from temperature changes," *Nature Geoscience*, vol. 1, no. 8, pp. 511–514, 2008.

[6] R. Yu and J. Li, "Hourly rainfall changes in response to surface air temperature over eastern contiguous China," *Journal of Climate*, vol. 25, no. 19, pp. 6851–6861, 2012.

[7] P. Zhai, C. Wang, and W. Li, "A review on study of change in precipitation extremes," *Climate Change Research*, vol. 3, no. 3, pp. 144–148, 2007.

[8] H. Zhang and P. Zhai, "Temporal and spatial characteristics of extreme hourly precipitation over eastern China in the warm season," *Advances in Atmospheric Sciences*, vol. 28, no. 5, pp. 1177–1183, 2011.

[9] J. Li, R. Yu, and W. Sun, "Duration and seasonality of hourly extreme rainfall in the central eastern China," *Acta Meteorologica Sinica*, vol. 27, no. 6, pp. 799–807, 2013.

[10] J. Li, R. Yu, and T. Zhou, "Seasonal variation of the diurnal cycle of rainfall in southern contiguous China," *Journal of Climate*, vol. 21, no. 22, pp. 6036–6043, 2008.

[11] R. Yu, Y. Xu, T. Zhou, and J. Li, "Relation between rainfall duration and diurnal variation in the warm season precipitation over central eastern China," *Geophysical Research Letters*, vol. 34, no. 13, Article ID L13703, 2007.

[12] R. Yu, T. Zhou, A. Xiong, Y. Zhu, and J. Li, "Diurnal variations of summer precipitation over contiguous China," *Geophysical Research Letters*, vol. 34, no. 1, Article ID L01704, 2007b.

[13] R. A. Maddox, C. F. Chappell, and L. R. Hoxit, "Synoptic and meso-α scale aspects of flash flood events," *Bulletin of the American Meteorological Society*, vol. 60, no. 2, pp. 115–123, 1979.

[14] V. Mishra, J. M. Wallace, and D. P. Lettenmaier, "Relationship between hourly extreme precipitation and local air temperature in the United States," *Geophysical Research Letters*, vol. 39, no. 16, Article ID L16403, 2012.

[15] C. Wasko, A. Sharma, and F. Johnson, "Does storm duration modulate the extreme precipitation-temperature scaling relationship?" *Geophysical Research Letters*, vol. 42, no. 20, pp. 8783–8790, 2015.

[16] Y. Luo, M. Wu, F. Ren, J. Li, and W.-K. Wong, "Synoptic situations of extreme hourly precipitation over China," *Journal of Climate*, vol. 29, no. 24, pp. 8703–8719, 2016.

[17] S. B. Shaw, A. A. Royem, and S. J. Riha, "The relationship between extreme hourly precipitation and surface temperature in different hydroclimatic regions of the United States," *Journal of Hydrometeorology*, vol. 12, no. 2, pp. 319–325, 2011.

[18] H. Wang, F. Sun, and W. Liu, "The dependence of daily and hourly precipitation extremes on temperature and atmospheric humidity over China," *Journal of Climate*, vol. 31, no. 21, pp. 8931–8944, 2018.

[19] P. Liang and Y. Ding, "The long-term variation of extreme heavy precipitation and its link to urbanization effects in Shanghai during 1916-2014," *Advances in Atmospheric Sciences*, vol. 34, no. 3, pp. 321–334, 2017.

[20] N. A. Lock and A. L. Houston, "Spatiotemporal distribution of thunderstorm initiation in the US Great Plains from 2005 to 2007," *International Journal of Climatology*, vol. 35, no. 13, pp. 4047–4056, 2015.

[21] Y. Guo and J. Sun, "Characteristics of strong convective wind events caused by three types of convective systems in Hubei province," *Chinese Journal of Atmospheric Sciences*, vol. 43, no. 3, pp. 483–497, 2019.

[22] R. Yang, Y. Zhang, J. Sun, and J. Li, "The comparison of statistical features and synoptic circulations between the eastward-propagating and quasi-stationary MCSs during the warm season around the second-step terrain along the middle reaches of the Yangtze River," *Science China Earth Sciences*, vol. 63, no. 8, pp. 1209–1222, 2020.

[23] I. Velasco and J. M. Fritsch, "Mesoscale convective complexes in the Americas," *Journal of Geophysical Research*, vol. 92, no. D8, pp. 9591–9613, 1987.

[24] A. G. Laing and J. M. Fritsch, "The global population of mesoscale convective complexes," *Quarterly Journal of the Royal Meteorological Society*, vol. 123, no. 538, pp. 389–405, 1997.

[25] E. J. Zipser, D. J. Cecil, C. T. Liu, S. W. Nesbitt, and D. P. Yorty, "Where are the most intense thunderstorms on earth?" *Bulletin of the American Meteorological Society*, vol. 87, no. 8, pp. 1057–1072, 2006.

[26] M. Schröder, M. König, and J. Schmetz, "Deep convection observed by the spinning enhanced visible and infrared imager on board meteosat 8: spatial distribution and temporal evolution over africa in summer and winter 2006," *Journal of Geophysical Research*, vol. 114, no. D5, Article ID D05109, 2009.

[27] U. Romatschke and R. A. Houze, "Extreme summer convection in South America," *Journal of Climate*, vol. 23, no. 14, pp. 3761–3791, 2010.

[28] K. L. Rasmussen and R. A. Houze, "Orogenic convection in subtropical South America as seen by the TRMM satellite," *Monthly Weather Review*, vol. 139, no. 8, pp. 2399–2420, 2011.

[29] S. Rafati and M. Karimi, "Assessment of mesoscale convective systems using IR brightness temperature in the southwest of Iran," *Theoretical and Applied Climatology*, vol. 129, no. 1-2, pp. 539–549, 2017.

[30] Y. Zheng, J. Chen, and P. Zhu, "Climatological distribution and diurnal variation of mesoscale convective systems over China and its surrounding areas in summer," *Chinese Science Bulletin*, vol. 53, no. 4, pp. 471–481, 2008.

[31] X. Qi and Y. Zheng, "Distribution and spationtemporal variations of deep convection over China and its vicinity during the summer of 2007," *Journal of Applied Meteorological Science*, vol. 20, pp. 286–294, 2009.

[32] T. M. Weckwerth, J. W. Wilson, M. Hagen et al., "Radar climatology of the COPS region," *Quarterly Journal of the Royal Meteorological Society*, vol. 137, no. S1, pp. 31–41, 2011.

[33] W. Xu and E. J. Zipser, "Diurnal variations of precipitation, deep convection, and lightning over and east of the eastern Tibetan plateau," *Journal of Climate*, vol. 24, no. 2, pp. 448–465, 2011.

[34] P. Fu, K. Zhu, K. Zhao, B. Zhou, and M. Xue, "Role of the nocturnal low-level jet in the formation of the morning precipitation peak over the Dabie Mountains," *Advances in Atmospheric Sciences*, vol. 36, no. 1, pp. 15–28, 2019.

[35] R. Yu, J. Li, H. Chen, and W. Yuan, "Progress in studies of the precipitation diurnal variation over contiguous China," *Acta Meteorologica Sinica*, vol. 72, no. 5, pp. 948–968, 2014.

[36] J. Sun and F. Zhang, "Impacts of mountain-plains solenoid on diurnal variations of rainfalls along the Mei-Yu front over the east China plains," *Monthly Weather Review*, vol. 140, no. 2, pp. 379–397, 2012.

[37] Z. Jiang, D.-L. Zhang, R. Xia, and T. Qian, "Diurnal variations of pre-summer rainfall over southern China," *Journal of Climate*, vol. 30, no. 2, pp. 755–773, 2017.

[38] M. Xue, X. Luo, K. Zhu, Z. Sun, and J. Fei, "The controlling role of boundary layer inertial oscillations in meiyu frontal precipitation and its diurnal cycles over China," *Journal of Geophysical Research: Atmospheres*, vol. 123, no. 10, pp. 5090–5115, 2018.

[39] Y. Zhang, M. Xue, K. Zhu, and B. Zhou, "What is the main cause of diurnal variation and nocturnal peak of summer precipitation in Sichuan Basin, China? The key role of boundary layer low-level jet inertial oscillations," *Journal of Geophysical Research: Atmospheres*, vol. 124, no. 5, pp. 2643–2664, 2019.

[40] Y. Du and R. Rotunno, "Diurnal cycle of rainfall and winds near the south coast of China," *Journal of the Atmospheric Sciences*, vol. 75, no. 6, pp. 2065–2082, 2018.

[41] Y. Du, Q. Zhang, Y.-L. Chen, Y. Zhao, and X. Wang, "Numerical simulations of spatial distributions and diurnal variations of low-level jets in China during early summer," *Journal of Climate*, vol. 27, no. 15, pp. 5747–5767, 2014.

[42] X. Li, N.-C. Lau, and T.-C. Lee, "An observational study of the diurnal variation of precipitation over Hong Kong and the underlying processes," *Journal of Applied Meteorology and Climatology*, vol. 57, no. 6, pp. 1385–1402, 2018.

[43] B. C. Bhatt and K. Nakamura, "A climatological-dynamical analysis associated with precipitation around the southern part of the Himalayas," *Journal of Geophysical Research*, vol. 111, no. D2, Article ID D02115, 2006.

[44] S. Yin, D. Chen, and Y. Xie, "Diurnal variations of precipitation during the warm season over China," *International Journal of Climatology*, vol. 29, no. 8, pp. 1154–1170, 2009.

[45] A. K. Blackadar, "Boundary layer wind maxima and their significance for the growth of nocturnal inversions," *Bulletin of the American Meteorological Society*, vol. 38, no. 5, pp. 283–290, 1957.

[46] J. R. Holton, "The diurnal boundary layer wind oscillation above sloping terrain," *Tellus*, vol. 19, no. 2, pp. 199–205, 1967.

[47] A. Shapiro, E. Fedorovich, and S. Rahimi, "A unified theory for the Great Plains nocturnal low-level jet," *Journal of the Atmospheric Sciences*, vol. 73, no. 8, pp. 3037–3057, 2016.

[48] Y. Du and G. Chen, "Heavy rainfall associated with double low-level jets over southern China. Part I: ensemble-based analysis," *Monthly Weather Review*, vol. 146, no. 11, pp. 3827–3844, 2018.

[49] G. Chen, R. Lan, W. Zeng, H. Pan, and W. Li, "Diurnal variations of rainfall in surface and satellite observations at the monsoon coast (South China)," *Journal of Climate*, vol. 31, no. 5, pp. 1703–1724, 2018.

[50] M. Wu and Y. Luo, "Mesoscale observational analysis of lifting mechanism of a warm-sector convective system producing the maximal daily precipitation in China mainland during pre-summer rainy season of 2015," *Journal of Meteorological Research*, vol. 30, no. 5, pp. 719–736, 2016.

[51] Z. Ren, Z. Zhang, C. Sun et al., "Development of three-step quality control system of real-time observation data from AWS in China," *Meteorlogical Monthly (in Chinese)*, vol. 41, no. 10, pp. 1268–1277, 2015.

[52] J. Chen, Y. Zheng, X. Zhang, and P. Zhu, "Distribution and diurnal variation of warm-season short-duration heavy rainfall in relation to the MCSs in China," *Acta Meteorologica Sinica*, vol. 27, no. 6, pp. 868–888, 2013.

[53] J. Chen, Y. Zheng, X. Zhang, and P. Zhu, "Analysis of the climatological distribution and diurnal varialions of the short-duration heavy rain and its relation with diurnal variations of the MCSs over China during the warm season," *Acta Meteorologica Sinica*, vol. 71, no. 3, pp. 367–382, 2013.

[54] L. Liu, Z. Ruan, and D. Qin, "A Case analysis of mesoscale structure of the Meiyu front rainstorm process in the Yangtze river basin," *Science in China - Series D: Earth Sciences*, vol. 34, no. 12, pp. 1193–1201, 2004.

[55] Y. Ni and X. Zhou, "Study for formation mechanism of heavy rainfall within the meiyu front along the middle and downstream of Yangtze river and theories and methods of their detection and prediction," *Acta Meteorologica Sinica*, vol. 62, no. 5, pp. 647–662, 2004.

[56] K. Ninomiya, "Large- and meso-α-scale characteristics of meiyu/baiu front associated with intense rainfalls in 1-10 july 1991," *Journal of the Meteorological Society of Japan*, vol. 78, no. 2, pp. 141–157, 2000.

[57] J. Wang and Z. Li, "Numerical simulation and diagnostic analysis on mesoscale convective systems of a torrential rain case in meiyu period of 1998," *Acta Meteorologica Sinica*, vol. 60, no. 2, pp. 146–155, 2002.